Supporting Information

Illing et al. 10.1073/pnas.1612964114

SI Text

The confinement of colloids to two dimensions is achieved by sedimentation to an interface, which in our case is the lower water/air surface in hanging droplet geometry. The volume is regulated actively with a microsyringe to get a flat interface. The fluid interface guarantees free diffusion of the colloids (without any pinning) within the horizontal monolayer, but the sedimentation height is about 20 nm and negligible compared with the size of the colloids. The latter consist of polystyrene beads with diameter $\sigma_A = 4.5\,\mu$m (species A) for the crystals and a mixture of species A and B (to avoid crystallization) for the glass samples. Species B has $\sigma_B = 2.8\,\mu$m and the glassy mixture has a relative concentration of $\xi = N_B/(N_A + N_B) \approx 50\,\%$, where N_A and N_B are the number of particles of both species in the field of view. The colloidal beads are further doped with iron oxide nanoparticles, which results in a superparamagnetic behavior and a mass density of 1.7 kg/dm^3. The whole monolayer consists of several hundred thousand particles, where $\approx$ 2000 particles are monitored by video microscopy in a $1158 \times 865\,\mu$m^2 subwindow in the glass sample and $\approx$ 3000 particles in a $835 \times 620\,\mu$m^2 subwindow in the crystalline sample. The individual colloids are tracked with a spatial resolution of $\approx$ 50 nm and with a time resolution of the order of a second. The system is kept at room temperature and exempt from density gradients due to a monthlong precise control of curvature and inclination of the interface.

Because of the superparamagnetic nature of the particles, the potential energy can be tuned by means of an external magnetic field $\vec{H}$ applied perpendicular to the monolayer, which induces a repulsive dipole–dipole interaction between the particles. The ratio between potential energy E_{mag} and diffusive thermal energy $k_B\,T$,

$$\Gamma = \frac{\mu_0}{4\pi} \cdot \frac{H^2 \cdot (\pi n)^{3/2}}{k_B\,T} (\xi \cdot \chi_B + (1-\xi) \cdot \chi_A)^2, \qquad \textbf{[S1]}$$

acts as inverse temperature (or dimensionless pressure for fixed volume and particle number). $n = 1/a^2$ is the 2D particle density with a mean particle distance $13\,\mu\text{m} < a < 22\,\mu$m (depending on the kind of sample). The magnetic susceptibility per bead is $\chi_A = 6.5 \cdot 10^{-11}$ Am^2/T and $\chi_B = 6 \cdot 10^{-12}$ Am^2/T for species A and B, respectively. For low Γ, the system is fluid because the thermal motion dominates. Increasing Γ induces crystallization at $\Gamma_m = 70$ (39) or dynamic arrest and vitrification at $\Gamma_G = 195$ (36). Digital image analysis gives the positions of the beads as a function of time. This provides the complete phase-space information of the colloidal ensembles at all relevant timescales on an "atomic" level. Our glasses are "well-aged"; we carefully checked that the α-process is independent of waiting time. Additional details of the 2D setup are described elsewhere (47). Using the water/air interface is crucial: We performed additionally a whole set of measurements as function of Γ on a solid substrate (object plate) where accidentally between 1 and 3% of particles were pinned. This pinning sufficiently suppresses Mermin–Wagner fluctuations and the differences between MSD and CR-MSD disappears, as shown in Fig. S1.

The 3D glass consists of monodisperse, charged polymethylmetacrylate (PMMA) particles of $\sigma_C = 2.6\,\mu$m diameter, covered with poly-12-hydroxystearic acid to prevent aggregation, which are dissolved in a well-adjusted cyclohexylbromide (CHB) and decaline mixture. This mixture matches the mass density to prevent sedimentation and simultaneously the refractive index of solvent and colloid. Because of the latter, the ensemble is not turbid, and one can look deep into the sample (which consists of several billion particles). The particles are doped with rhodamine 6G, and by using standard confocal microscopy, the 3D trajectories of up to 6000 particles can be monitored and analyzed simultaneously in a field of view of approximately $70 \times 60 \times 30\,\mu$m^3. Care has to be taken to use thoroughly cleaned solvents. CHB was passed through an activated alumina column to remove H_2O, HBr, and any other polar molecules and ions (48). Dispersed in CHB, PMMA colloids acquire a moderate positive charge. This seems to originate from the adsorption of protons and bromide ions stemming from the decomposition of CHB (with protons being adsorbed more likely) (49). Together with the small abundance of ions in the solvent, one obtains a screened Coulomb interaction with the dimensionless Yukawa potential:

$$u(r) = l_B \left(\frac{e^{\kappa/2}}{1 + \kappa\sigma_C/2} \right)^2 Z_{\text{eff}}^2 \cdot \frac{e^{-\kappa r}}{r}, \qquad \textbf{[S2]}$$

where κ is the inverse screening length of the ions and $l_B = e^2/(k_B\,T \cdot 4\pi\epsilon_0\epsilon_r)$ is the Bjerrum length. This is the length where the interaction potential between two elementary charges e in the medium with dielectric constant ϵ_r equals the thermal energy $k_B\,T$ (ϵ_0 is the dielectric constant of the vacuum). System parameters are determined from fits of theoretically computed structure factors $S(q)$ [using an approximate integral equation theory (50)] to the experimental data. The effective mean charge $Z_{\text{eff}} = 500$ on the surface of the colloid is the same for all three presented systems. Thus, the phase diagram has two relevant parameters left that counteract: These are the packing fraction Θ, which is given by the particle distance (and size), and the screening length κ^{-1}, given by the density of counterions and any other ions. The charge polydispersity ΔZ is dominated by the surface area polydispersity, thus being of the order of up to 17% for a size polydispersity determined by electron microscopy to be $\sim$8%. This effectively suppresses crystallization, which occurs not earlier than 1–2 wk after rejuvenation of the sample by shaking. Table S1 shows the parameters of three different glasses.

In the following, we will also compare experimental results with simulations. Those are made for a 2D binary mixture of hard disks undergoing Brownian motion by using an event-driven simulation algorithm (51, 52). The system contains $N = 16{,}000$ particles, is made up of a 50:50 mixture with diameters $d_{\text{A}} = 1$, $d_{\text{B}} = 1.4$, and is equilibrated by Newtonian dynamics before data are collected. The packing fraction ϕ, giving the ratio of the area occupied by the disks to the area of the system, varies from $\phi = 0.77$ to $\phi = 0.81$, hence in the vicinity of the glass transition point $\phi_{\text{c}} \approx 0.795$ (53). For the simulations, the averaging (angular brackets) is done for typically 100 runs as function of density and for finite size effects up to 200 independent runs as function of system size. Fig. S2 shows the comparison of MSD and CR-MSD in similar manner as Fig. 2 for the experimental systems.

We observed Mermin–Wagner fluctuations in 2D crystal and 2D glass. This raises the question of which low-dimensional systems will show Mermin–Wagner fluctuations. Because well-defined neighbor distances with low variance as in glasses, quasicrystals, and crystals are required, we suggest hyperuniformity, originally formulated to characterize structures with isotropic photonic bandgaps (54, 55), to be a necessary requirement: in hyperuniform structures the number variance $\sigma(R) = \langle N_R^2 \rangle - \langle N_R \rangle^2$ of N_R atoms within a n-dimensional sphere of radius R is proportional to the $n-1$ dimensional surface of the sphere.

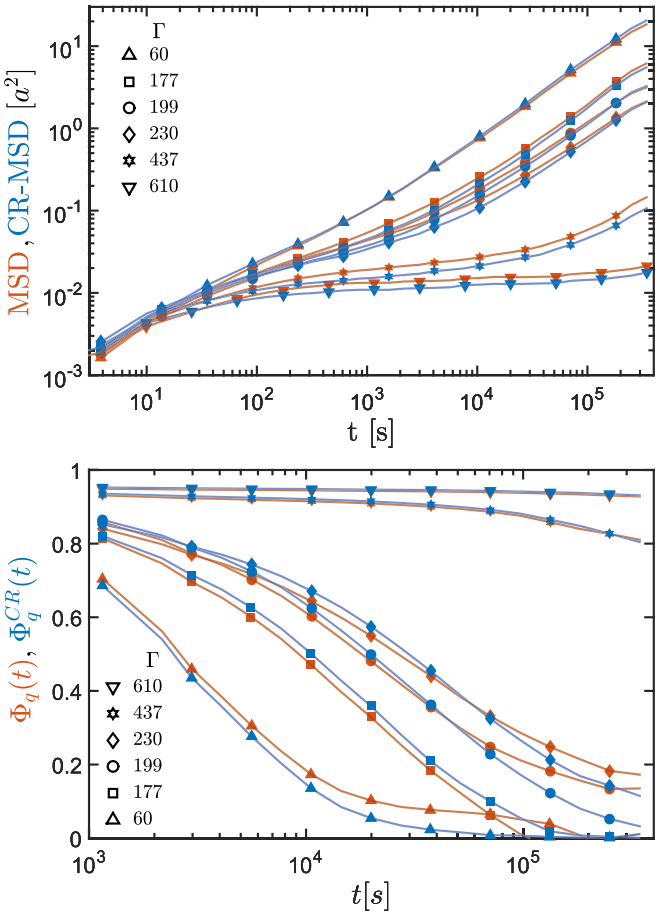

Fig. S1. (*Upper*) MSD of a colloidal monolayer on a solid substrate. Accidentally, between 1 and 3% of particles were pinned to the substrate, which efficiently suppresses Mermin–Wagner fluctuations. The upper two curves are fluid; the circles indicate a system close to the glass transition, whereas the lower three curves are solid. *Lower* shows the density correlator (main text) for the same system (again, $qa = 2\pi$).

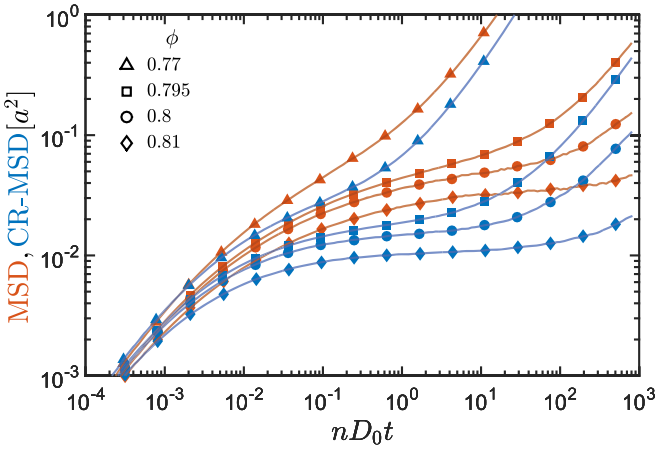

Fig. S2. The separation of MSD (red) and CR-MSD (blue) for the hard disk system shows Mermin–Wagner fluctuations. The triangles indicate a fluid system; the squares indicate a system with critical packing fraction; and the circles and diamonds show a solid sample. The data are the same as for the density correlator in Fig. 3, except for the fluid data.

Table S1. Parameters of the 3D glass

	Θ [%]	κ^{-1} [a_0]	Z_{eff}
Glass 1	21.5	0.183	500
Glass 2	19.2	0.176	500
Glass 3	19	0.166	500